International Journal of Modern Physics C, Vol. 11, No. 3 (2000) 493–517

STATIC PROPERTIES AND WAVEGUIDE MODES OF A WIDE LATERAL WINDOW JOSEPHSON JUNCTION*

JEAN-GUY CAPUTO

Laboratoire de Mathématiques, Institut de Sciences Appliquees and U.R.A. C.N.R.S. 1378, BP8, 76131 Mont-Saint-Aignan Cedex, France

NIKOS EFREMIDIS, NIKOS FLYTZANIS, and NIKOS LAZARIDES

Physics Department, University of Crete, 71409 Heraklion, Greece

YURI GAIDIDEI

Institute for Theoretical Physics, 252143 Kiev, Ukraine

IRENE MOULITSA and EMMANUEL VAVALIS

Mathematics Department, University of Crete, 71409 Heraklion, Greece and Institute of Applied and Computational Mathematics, FORTH 71110 Heraklion, Greece
E-mail: *mav@n208hp.cc.uch.gr*
E-mail: *mav@dafne.math.uch.gr*

Received 14 December 1999
Revised 13 March 2000

We developed an efficient hybrid mode expansion method to study the maximum tunneling current as a function of the external magnetic field for a 2D large area lateral window junction. We consider the inhomogeneity in the critical current density, which is taken a piecewise constant. The natural modes of the expansion in y, are the linearized eigen-modes around a static solution which satisfies the 1D sine-Gordon equation with the critical current variation in y, and the boundary conditions determined by the overlap component of the bias current, which can be inline or overlap like. The magnetic field along with the inline component of the bias current enters as a boundary condition on the modal amplitudes. We obtain fast convergent results and for a ratio of idle to window widths of $w_0/w = 4$ (in units of λ_J), only two modes are needed. A simple scaling is obtained for the maximum tunneling current as we vary the idle region width. We also present the linear electromagnetic waveguide modes taking into account the variation normal to the waveguide of the critical current and the capacitance.

Keywords: Josephson Junctions; Partial Differential Equations; Solitons.

PACS Nos.: 03.40.Kf, 05.40.+j, 66.90.+r, 42.25.-p.

Part of this work was supported by EEC grant SC1-CT91-0760 and a PENED grant (No. 2028/1995).

1. Introduction

The interpretation of the junction electrodynamics is useful both for the junction characterization and its exploitation in device design with the desired electromagnetic properties when an external magnetic field is applied.[1] For short junctions, it is easy to infer such properties as the critical Josephson current density J_c and the characteristic Josephson penetration length λ_J from I_0, the maximum current at zero field, and H_c, the critical field above which the Meissner-like state for flux penetration breaks i.e., $I_{\max}(H_c) = 0$ in the (0–1) fluxon branch. For large area junction parameters, one must fit the whole experimental maximum current pattern, since 1D estimations can lead to erroneous parameters, due to self-field effects that give the complex patterns.

The situation is more complicated in the so called window junctions which is the produced device of the most modern layer-by-layer production techniques. In Ref. 2, we saw that the idle (for tunneling) region surrounding the tunneling window, influences the fluxon width and therefore, the characteristic scale of the magnetic flux variation. Thus, one can say that both the idle region[2] and the geometry[3] introduce a new characteristic length λ_{eff}. At the same time, the two dimensionality of the problem requires a numerical solution with heavy computation. In Ref. 4, an efficient mode expansion method was used for the study of the large area junction with homogeneous properties over the whole surface. It was applied for the case of a pure 2D sine-Gordon system that corresponds to zero idle region. Here, we extend the method to the case where, there is a lateral idle region along the long sides of a rectangular junction, so that we still preserve the homogeneity in the x-direction. This extension requires the calculation of new expansion modes in the y-direction whose form depends on the variation of the properties of the junction physical along the waveguide width. The $x-y$ uncoupling follows the homogeneity of the waveguide in the x-direction, and the fact that we look for traveling waves in the x-direction. This simplification is of great analytical help, while keeping the dominant influence of the idle region. It also gives a simple way to take into account, not only the inhomogeneity in the critical tunneling current, but also in the inductive properties of the films in an efficient and accurate manner.

It is well known that, the 1D sine-Gordon equation has the linear modes with a dispersion relation $\omega(k)^2 = 1+k^2$ (with unity linear wave velocity) with a gap below $\omega(0) = 1$. On the other hand, a simple (no tunneling) dielectric waveguide with width w_0 will have many branches, which in the long wavelength limit (standing waves along y) are separated by $\Delta\omega = c_i\pi/w_0$, where c_i is the linear velocity in the passive waveguide and for a 2D junction (no lateral region), the modes are at $\omega_n(0) = \sqrt{(1 + (n\pi/w)^2)}$. So, in the limit $w_0 \to 0$, only the lowest mode need to be considered as for the 1D sine-Gordon. Our lateral window junction can be considered as a parallel array structure of two passive waveguides with an active one in between. This coupling introduces strong dispersion both due to the different tunneling properties, and the variation of the linear speed with the capacitance distribution along the width of the waveguide. The knowledge of the spectrum of

the modes is useful, both for the dynamic properties of fluxons and as a source of high frequency Cherenkov type radiation, when the velocity of the magnetic flux matches the phase velocity of some linear waves. These modes will be calculated in the limit of no losses, which is well satisfied for frequencies less than twenty times the plasma frequency, which in our case is taken as unity.

In Sec. 2, we briefly describe the model and present the Split Mode method, where the coupling between x and y is treated in a mode expansion which transforms the 2D PDE problem into a system of ODE problems. In Sec. 3, we discuss the variation of the effective characteristic length with the junction geometric parameters. In Sec. 4, we present the numerical results for both the inline and overlap geometry for the case of critical current inhomogeneity. In Sec. 5, we present the dispersion relation for linear modes. In the final section, we summarize our results.

2. Model and Expansion Method

We consider the case of a long and wide window junction (length ℓ and width w) with the lateral idle region symmetrically placed for $w/2 < |y| < w_0/2$. The length is measured in units of λ_J, the characteristic Josephson length in the isolated window,[1] $\lambda_J = \sqrt{\phi_0/J_c\mu_0 d_0}$, where d_0 is the magnetic thickness of the junction so that $\mu_0 d_0$ is the inductance, ϕ_0 is the quantum of the flux and J_c is the critical current density in the window region.

The static properties of the junction are described by the inhomogeneous 2D static sine-Gordon equation for the phase difference $\phi(x, y)$ i.e.,

$$\frac{\partial^2\phi}{\partial x^2} + \frac{\partial^2\phi}{\partial y^2} = -U(y)\sin\phi\,, \tag{1}$$

where,

$$U(y) = \begin{cases} -1 & |y| \le w/2 \qquad \text{window region} \\ 0 & w/2 \le |y| \le w_0/2 \quad \text{idle region}\,. \end{cases} \tag{2}$$

Equation (1) is the conservation of the current flow in the surface of the superconducting films, and the tunneling current across the barrier in the dimensionless quantities. The surface currents are defined from the gradient of the phase, in the units of $\phi_0/\mu_0 d_0\lambda_J$, which is also related to the local magnetic field $\mathbf{H}$, as $\boldsymbol{\nabla}_{x,y}\phi = (\hat{\mathbf{z}} \times \mathbf{H})$, where $\mathbf{H}$ is in units of $\phi_0/\mu_0 d_0$, and $\hat{\mathbf{z}}$ is a unit vector normal to the superconducting films. The boundary conditions (BC) at the outside perimeter C with normal $\hat{\mathbf{n}}$ towards the outside are, $\hat{\mathbf{n}} \cdot \nabla\phi|_C = \hat{\mathbf{n}} \cdot (\hat{\mathbf{z}} \times \mathbf{H})|_C$, where $\mathbf{H}$ is the total magnetic field due to bias or the external magnetic field and they are explicitly written as:

$$\left.\frac{\partial\phi}{\partial x}\right|_{x=\pm\ell/2} = H_e \pm \frac{I_{\text{in}}}{2w_0}\,, \tag{3}$$

$$\left.\frac{\partial\phi}{\partial y}\right|_{y=\pm w_0/2} = \pm\,\frac{I_{\text{ov}}}{2\ell}\,. \tag{4}$$

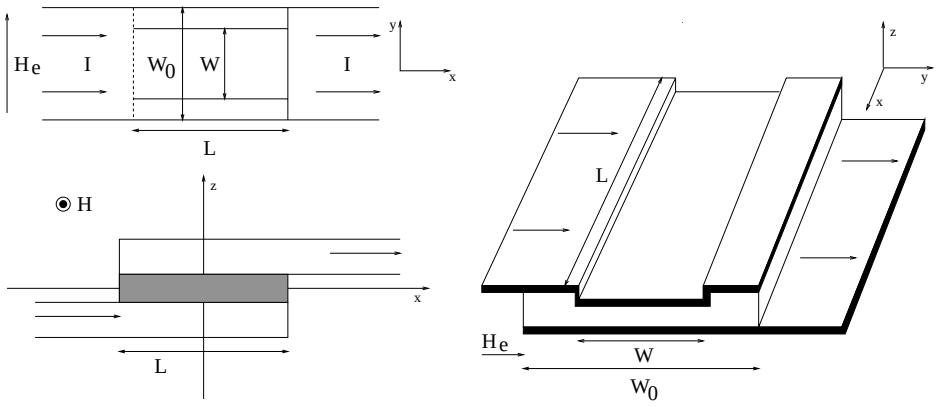

(a) (b)

Fig. 1. Schematic diagrams of the lateral idle window junctions with (a) inline and (b) overlap geometries. In (a), we show a view from above (top) and a vertical cross-section at $y = 0$. The dashed line in (a) denotes that the left electrode is in the lower superconducting film.

If $I_{\rm ov} = 0\,(I_{\rm in} = 0)$, we have the inline (overlap) BC correspondingly (see Fig. 1), while if both $I_{\rm in}$ and $I_{\rm ov} \neq 0$, we can also study the case where the bias current is peaked near the corners, and in this case the total current is $I = I_{\rm ov} + I_{\rm in}$.

For the solution of the problem, we use a split Fourier expansion by introducing an auxiliary function $\phi_0(y)$, which satisfies the 1D static equation.

$$\frac{d^2\phi_0(y)}{dy^2} = -U(y)\sin\phi_0(y) \tag{5}$$

with the boundary conditions along the lateral boundary in Eq. (4), so that,

$$\left.\frac{d\phi_0(y)}{dy}\right|_{y=\pm w_0/2} = \frac{I_{\rm ov}}{2\ell}\,, \tag{6}$$

where $I_{\rm ov}$ is the current input along the lateral sides. When this is zero, then $\phi_0(y) = 0$ or π, otherwise, the solution is given explicitly in terms of elliptic functions.[4,5]

Then, we use the expansion,

$$\phi(x,y) = \phi_0(y) + \sum_{n=1}^{\infty} A_n(x)X_n(y) \tag{7}$$

where the complete set of the orthonormal functions $X_n(y)$, are the eigenmodes around the static solution $\phi_0(y)$, and satisfy,

$$-X_n''(y) - U(y)\cos\phi_0(y)X_n(y) = \lambda_n X_n(y)\,, \tag{8}$$

with homogeneous BC, so that, $X_n'(\pm\, w_0/2) = 0$, where " $'$ " denotes the differentiation with the corresponding variable. For the case of zero lateral current where, $\phi_0 = 0$, the eigenvalue problem reduces to that of a square barrier for which analytic

solutions are given in the Appendix. It is easy, by direct substitution of Eq. (7) in Eq. (1) and using Eqs. (5) and (8), to obtain the equations for the modal amplitudes $A_n(x)$ in the general form.

$$A_m''(x) - \lambda_m A_m(x) - \sum_{n=1}^{\text{nmodes}} \left\{ \int_{-w_0/2}^{w_0/2} U(y) \cos\phi_0(y) X_n(y) X_m(y) dy \right\} A_n$$
$$= - \int_{-w_0/2}^{w_0/2} dy U(y) X_m(y) \left\{ \sin\left(\phi_0(y) + \sum_{n=1}^{\text{nmodes}} A_n(x) X_n(y) \right) - \sin\phi_0(y) \right\}, \tag{9}$$

where, nmodes is the number of modes kept in the expansion. For simplicity in the presentation, in the sequel, we will not give explicitly the arguments of $A_n(x)$ and $X_n(y)$.

In the inline geometry, the problem is simplified because the eigenmodes $X_n(y)$ are independent of the external field and current, and depend only on the widths of the window and idle regions. Since in that case, $\phi_0(y) = 0$, the equations for the amplitudes $A_m(x)$ are simplified to:

$$A_m'' - \lambda_m A_m + \sum_{n=1}^{\text{nmodes}} \left\{ \int_{-w/2}^{w/2} X_n X_m dy \right\} A_n$$
$$= + \int_{-w/2}^{w/2} dy X_m \left\{ \sin\left(\sum_{n=1}^{\text{nmodes}} A_n X_n \right) \right\}. \tag{10}$$

If $\phi_0(y) = \pi$ is chosen, then in Eq. (8), the potential is a square well and the sign of the integral terms in Eq. (10) is negative. A useful remark is that, there is no linear coupling between the different A_n's and the coupling comes only in the nonlinear terms. This means that the width will be determined by the coefficient of the linear term corresponding to the most dominant mode, which in our case is λ_1.

The eigenvalues of the linear problem in Eq. (8) are not only the numerically useful quantities, but have a physical meaning also. They give the frequencies $\omega_n(k = 0)$ of the long wavelength electromagnetic waves that can propagate in the junction along the x-direction, in the absence of external current and magnetic field. These will be discussed further in Sec. 5.

In the limit $w = w_0$ (no passive region), the eigenvalues from [Eq. (33)] are $\lambda_n \equiv \kappa_n^2 = 1 + [2(n-1)\pi/w)]^2$, which simply says that, in the absence of the idle region, the symmetric modes correspond to an integer number of wavelengths in the y-direction, and the unity comes from the tunneling, and does not exist in the opposite limit with $w = 0$ (no window). In that case, we get the pure waveguide modes, $\lambda_n = [2(n-1)\pi/w)]^2$. The corresponding wavelength in the x-direction is infinite. In the case of $w_0 = w \to 0$, the separation between the eigenvalues goes to infinity, so that only the lowest one needs to be considered, i.e., $\lambda_1 = 1$. This is

the long wavelength mode of the usual sine-Gordon dispersion relation $\omega^2 = 1 + k^2$, where k is the wavevector in the x-direction.

3. Effective λ_J and Soliton Width

The lateral idle region has an effect on the structure of the soliton and in particular on its width. For a narrow idle region, one can use the approximate expression for a window centered fluxon,

$$\phi = 4 \arctan \exp\left(-\frac{x - x_m}{d(y)}\right), \tag{11}$$

where we use a y-dependent width $d(y)$. Under certain conditions, the variation of $d(y)$ with y is small, and then one can define an average half-width which can be determined by the energy minimization[6] to be equal to:

$$d_i^0 = \sqrt{\frac{w_0}{w}} = \sqrt{1 + \frac{2w'}{w}}, \tag{12}$$

if the idle region is small with $w' = (w_0 - w)/2$. The case of a long window in an infinite idle region can also be treated analytically[2] using conformal mapping and an analogy with two plate capacitors to give,

$$d_i^\infty = \frac{\pi}{2}\frac{1}{w}\left[1 + \sqrt{1 + \frac{4w^2}{\pi^2}}\right]. \tag{13}$$

This formula can be derived under the condition that, $d(y)$ varies slowly within the window, which is the case if $w/\lambda_J < 1$.[2]

We applied our approach to study the fluxon width by placing it at the center with no external current and magnetic field. We remark that for a finite junction, this situation is neutrally stable and therefore, it is important in the numerical scheme to preserve the symmetry of zero net force, i.e., even the rounding errors should not cause a small force. For this reason, we chose $\phi_0(y) = \pi$, so that $\cos\phi_0 = -1$, and the equations for A_n are as in Eq. (10), except for a sign change in the last two terms.

For small w and w' (or $w_0 \approx w$), only one mode is sufficient and the eigenfunction is almost constant within $|y| < w/2$. Then, the equation for $A_1(x)$ is approximated as:

$$A_1'' - \lambda_1 A_1 + w X_1^2(0) A_1 = w X_1(0)\{\sin(A_1 X_1(0))\}. \tag{14}$$

If we expand the sine term, then, we can keep the first two terms up to A_1^3 which is a reasonable approximation for the solution near the center. It can be seen that in this case, the half-width of the solution is determined by the coefficient of the linear term, i.e., the eigenvalue λ_1 (with the width given by $D = \sqrt{1/\lambda_1}$) in Eq. (8),

which is obtained from the lowest root of:

$$\sqrt{1-\kappa_n^2}\tan\left(\sqrt{1-\kappa_n^2}\frac{w}{2}\right) = -\kappa_n \tanh\left[\frac{\kappa_n}{2}(w-w_0)\right], \tag{15}$$

where, we put $\lambda_n = \kappa_n^2$. Note that, because of the symmetry of the problem, we are interested only in the eigenvalues of the symmetric modes. It is easy to see that for small w and w', $\lambda_1 = w/w_0$ and thus, we recover the result of Eq. (12), which shows that, for this case only, the lateral idle region is important. If w is small, the higher eigenvalues $\lambda_n \sim (2\pi(n-1)/w)^2 (n > 1)$ are very high in value so that, as seen in Eq. (10), the corresponding amplitude has to be small since the other terms are small (bounded).

Another situation for which an approximate analytic result is possible, is the limit $w_0 \to \infty$ for which the eigenvalue is given from $\sqrt{1-\kappa_n^2}\tan[\sqrt{1-\kappa_n^2}(w/2)] = \kappa_n$. If we define $\kappa = \sin\theta$, we can solve and obtain $\theta/\cos\theta = w/2$. If $w \ll 1$, then $\theta \approx w/2$ and the estimation for the width is $D = 2/w$. This gives the right dependence on w as in Eq. (13), but with a different factor. It is true that, it is the lateral part that gives the main effect and therefore, the $1/w$ dependence, but the possibility of the lines of constant phase closing around the ends can increase the fluxon width. We must remember that Eq. (13) was derived for a very narrow window with the idle region all around and the factor difference is not unexpected. Another reason for the difference is that, due to the large idle region, one needs an increased number of normal modes in the expansion.

If we consider $w/2 \gg 1$, but still $w \ll w_0$, then put $\theta = \pi/2 - \bar{\theta}$, to obtain $\lambda_1 = 1/(1+\pi^2/2w^2)$. In this case, the width (assumed to be uniform) is:

$$D \approx (1+\pi^2/2w^2)\,.$$

Next, we give numerical estimates for a case of realistic experimental dimensions. In Fig. 2, we present our numerical results for the half-width, $D(y=0)$ for a (10×1) window as a function of w_0. The dotted curve is the result of the simple expression in Eq. (12), while we see that, even for $w_0 = 4$, only three modes (crosses in Fig. 2) are sufficient to converge to a result which is not very far from the dotted curve. Actually, the agreement is even better if we had plotted the average width over y. In fact, the surprise is that it is so close even though the ratio $w_0/w = 4$. The main reason for this is that, the nonlinearity of the problem does not allow any significant curving of the constant phase lines in distances less than some characteristic length which for the pure window is λ_J, but for the window junction, is of the order of D, which can be considered as λ_{eff}. Examining Eq. (11), we can conclude that it is reasonable to average the half-width over the window width w. The variation of $D(y)$ was less than 5% even for the largest w_0. Thus, the average value will be even closer to the analytic result. For our case, the new width D can be considered as an effective Josephson length to normalize the junction dimensions.

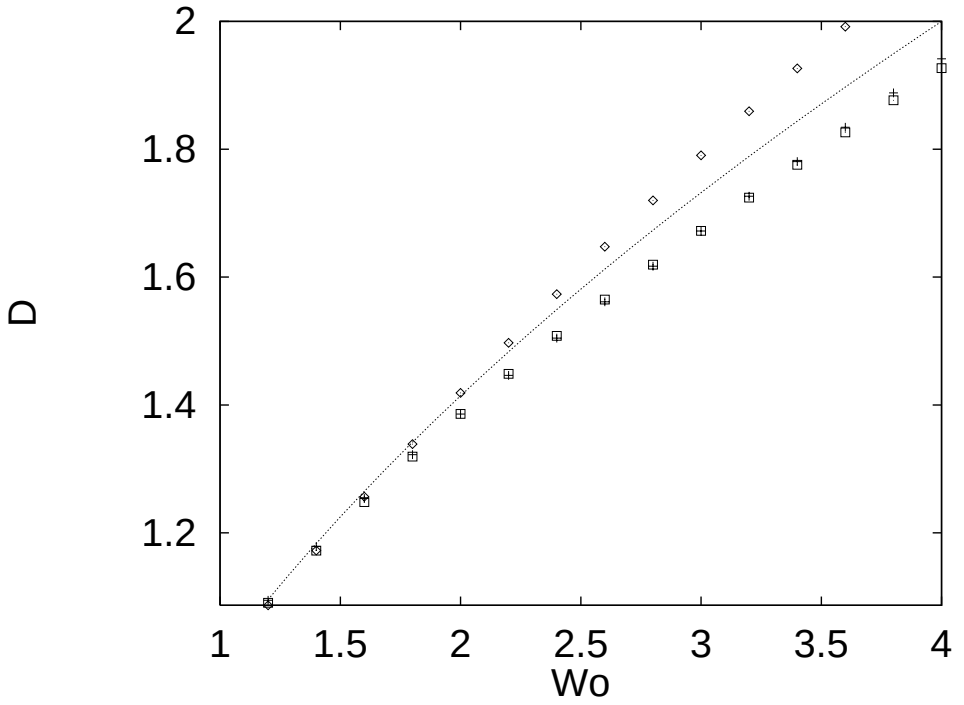

Fig. 2. Plot of static fluxon width as a function of idle region size w_0 by including 1 (diamonds), 3 (crosses), and 4 (squares) eigenmodes. Dotted line is from the analytic result in Eq. (12).

4. Maximum Current versus External Magnetic Field

The application of an external magnetic field on a Josephson junction, induces self fields which tend to oppose the entrance of the magnetic field from the ends in an analog way as the Meissner effect for the bulk superconductor. This has an effect that the maximum current that can tunnel through the junction also changes. This variation for short junctions or for temperatures near the critical superconducting temperature T_c, is the simple Fraunhofer diffraction pattern. For lengths $\ell \ll \lambda_J$, the maximum current depends on besides the magnetic field, also on the window dimensions and form, as well as on the idle region geometry.[3] It also depends very strongly on the existence of defects. Thus, the experimental measurement of the $I_{\max}(H)$ plot can help to characterize the quality of the junction. It can also determine the parameters of the junction J_0 and λ_J. For a short junction, this is straight forward from the maximum current at zero external field and the critical field where $I_{\max}$ vanishes, and above H_c, the external flux enters the length of the junction. For a longer junction, one can only do it by fitting the experimental data. In fact, measurement of $I_{\max}(0)$ and H_c for inline current feed is not sufficient to characterize the junction, since there are three parameters for the perfect junction, i.e., J_0, d_0 and λ_{eff}. For a perfect junction, one can do the measurements at two temperatures $T = 0$ and near T_c for both inline and overlap bias current cases. If the junction

barrier has defects, then one has a difficult task to guess the form of the defects, he can get some help though from LTSTM measurements.[7] Also in some applications, one is interested to work with low maximum currents but also low external fields, this can be achieved by a geometry choice.

The maximum tunneling current $I_{\max}$ is a useful quantity since for slightly higher bias currents, the Josephson device switches from the pair tunneling to the quasiparticle mode for a given external magnetic field. This switching property can be exploited in several devices.

The knowledge of H_c, i.e., the value of the magnetic field for which the maximum tunneling current vanishes is also important for the flux flow operation, since the external magnetic field (with $H_e > H_c$) fixes the squeezed soliton separation and therefore, the frequency of emitted radiation when the fluxons reach the other end from the one they are introduced by the magnetic field.

4.1. *Inline geometry*

In this case, we have $I_{\text{ov}} = 0$ and $I_{\text{in}} = I$. Even in the inline geometry [see Fig. 1(a)], the problem loses its 1D behavior due to the idle region. Since there is no current input along y, we have $\phi_0(y) = 0$. This choice is more appropriate than π since in the center (at $x = 0$) for a long window, $\phi(x)$ is close to zero. Also, the first eigenmode has the correct form decaying inwards as the Meissner-like effect requires. The choice $\phi_0(y) = 0$, gives the same results as for $\phi_0(y) = \pi$, but shows better convergence. The eigenmodes $X_n(y)$ can be obtained analytically and in Fig. 3, we show the first four for $w = 1$ and $w_0 = 4$. Due to the symmetry of the boundary

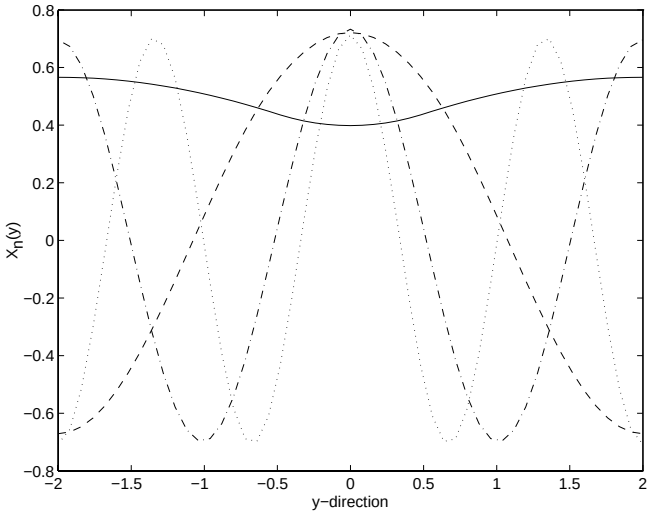

Fig. 3. Eigenmodes $X_n(y)$ with $n = 1 - 4$ for the inline geometry (independent of current) for $w_0 = 4$, $n = 1$ (continuous line), $n = 2$ (long dashed line), $n = 3$ (short dashed line), and $n = 4$ (dotted line).

conditions, we kept only the symmetric eigenmodes, while for the odd eigenmodes, the modal amplitudes vanish. If there was no idle region, the modes would be simple cosine modes of the form $\cos(2\pi(n-1)/w)$. In fact, only the first two modes differ significantly from the cosine form. Since for the inline geometry, $\phi_0(y)$ is independent of the bias current, the eigenmodes depend only on the parameters w and w_0. The modal amplitudes are obtained from Eq. (10) with the BC.

$$\left.\frac{dA_m}{dx}\right|_{x=\pm\ell/2} = \left(H \pm \frac{I}{2w_0}\right) \int_{-w_0/2}^{w_0/2} X_n(y)dy\,. \tag{16}$$

In Fig. 4, we plot the maximum tunneling current as a function of the external magnetic field in the inline geometry for three values of $w_0 = 1.2$, 2.0, and 4.0. The increase of the maximum current at zero magnetic field with w_0 is easily understood if we keep in mind the increase of the effective Josephson length. The shift of the H_c value for zero tunneling current is also easy to understand because, at that point we have exactly the penetration of one unit of the magnetic flux. The length over which magnetic flux penetrates at the edges is proportional to λ_{eff}. Thus, for an increase of w_0 (which increases the characteristic length), we obtain a decrease of H_c. In fact, using the numbers for λ_{eff} from Fig. 1, we get the H_c within 5%.

In Fig. 5, we plot the H_c as a function of the inverse of the effective length $1/D$, and as expected we get almost a straight line with the correct slope close to 2. In Fig. 6, we plot the maximum tunneling current at zero external field as a function of D, which was obtained for different w_0 values. By looking at Fig. 4, one can obtain

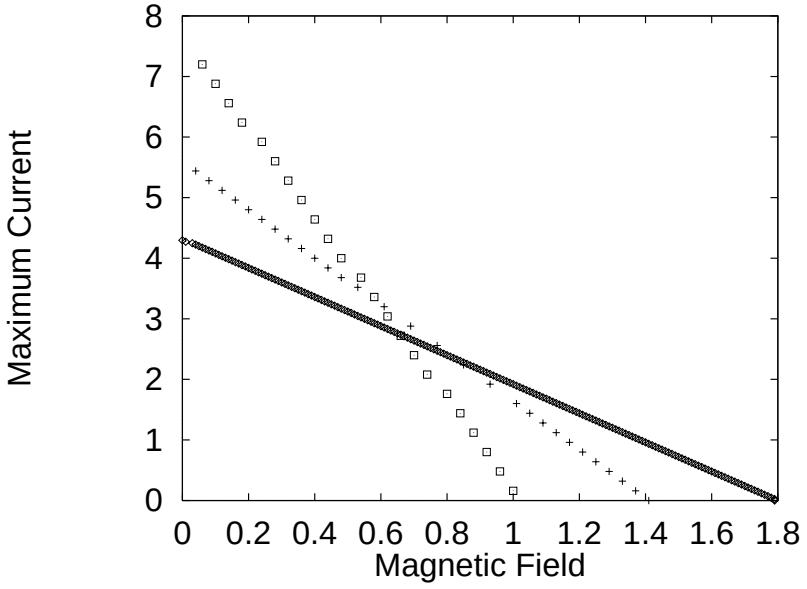

Fig. 4. Plot of the maximum tunneling current as a function of the external magnetic field for three different values of $w_0 = 1.2$ (rhombus), 2 (crosses), and 4 (squares).

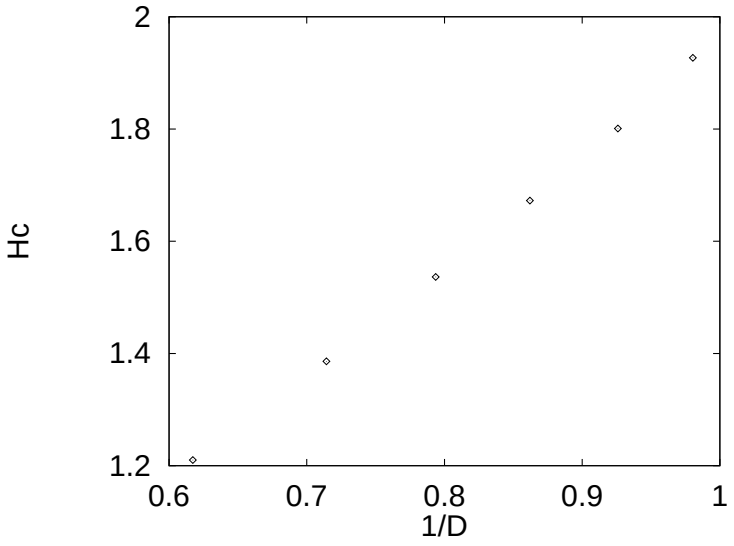

Fig. 5. Plot of the critical field H_c as a function of the inverse of the effective length $1/D$ obtained from Fig. 2 for different w_0.

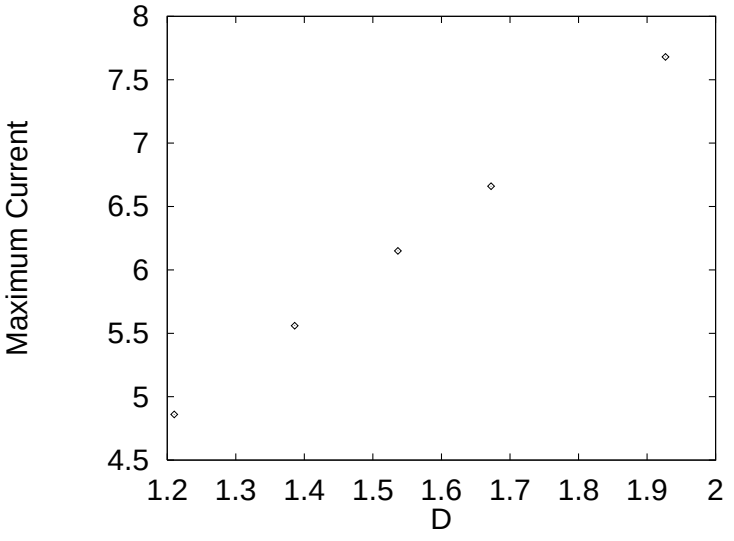

Fig. 6. Plot of the maximum tunneling current at $H = 0$ as a function of the effective length D obtained from Fig. 2 for different w_0.

$I_{\max}(0)$ as a function of w_0. Again, we see in Fig. 6, a linear relation with a slope of about 4.0 instead of w_0, the horizontal axis is $D(w_0)$. This is expected since the area over which the current tunnels is proportional to the effective Josephson length, D. For larger w_0, there will be deviations since the current enters the window from all sides.

4.2. *Overlap geometry*

In this case, we have $I_{\rm in} = 0$ and $I_{\rm ov} = I$ [see Fig. 1(b)]. Since in the idle region, the function satisfies $d^2\phi_0(y)/dy^2 = 0$, the boundary conditions at $y = \pm w_0/2$ can be applied at the internal boundary (on $y = \pm w/2$) and the solution for $\phi_0(y)$ is given by[4,5]:

$$\sin\phi_0 = \begin{cases} 2\sqrt{mm_1}cd(y|m)nd(y|m)\,, & |y| < \dfrac{w}{2}\,, \\ \sin\left(\dfrac{I}{2}\left(|y| - \dfrac{w}{2}\right) + \gamma\right)\,, & \dfrac{w}{2} < |y| < \dfrac{w_0}{2}\,, \end{cases} \tag{17}$$

where cd and nd are the elliptic functions with modulus m,[8] which is determined from the external current through the boundary condition,

$$2\sqrt{mm_1}sd\left(\frac{w}{2}\middle|m\right) = \frac{I}{2\ell}\,. \tag{18}$$

The constant γ is determined by matching the solutions at the interface between the idle and window regions, since the nonlinearity in the window completely determines the solution inside.

The corresponding eigenmodes must be obtained numerically and in Fig. 7, we plot the first four ($n = 1 - 4$) for $w_0 = 4.0$ and the maximum current that occurs for $H = 0.01$. In comparing with Fig. 3, we see that the only difference is with the lowest mode, except for an unimportant sign change. In this case, the lowest mode is almost flat and its corresponding eigenvalue is very close to zero. This is because the current is close to the maximum possible value in 1D, where an eigenfrequency

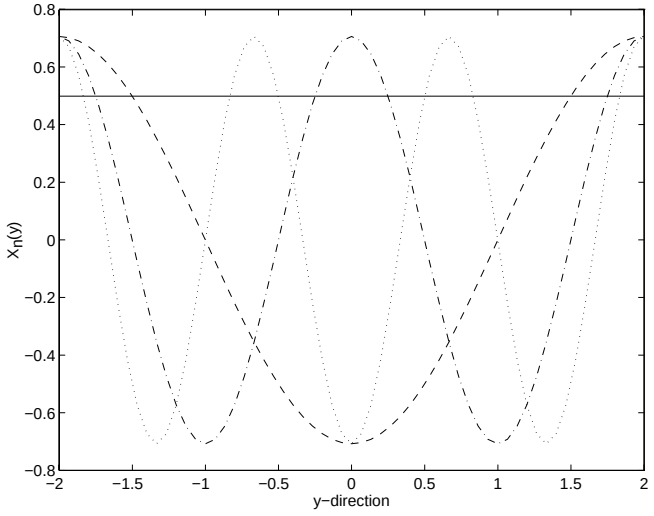

Fig. 7. Eigenmodes $X_n(y)$ with $n = 1 - 4$ for the overlap geometry at the maximum current for $H = 0.01$, and $w_0 = 4$.

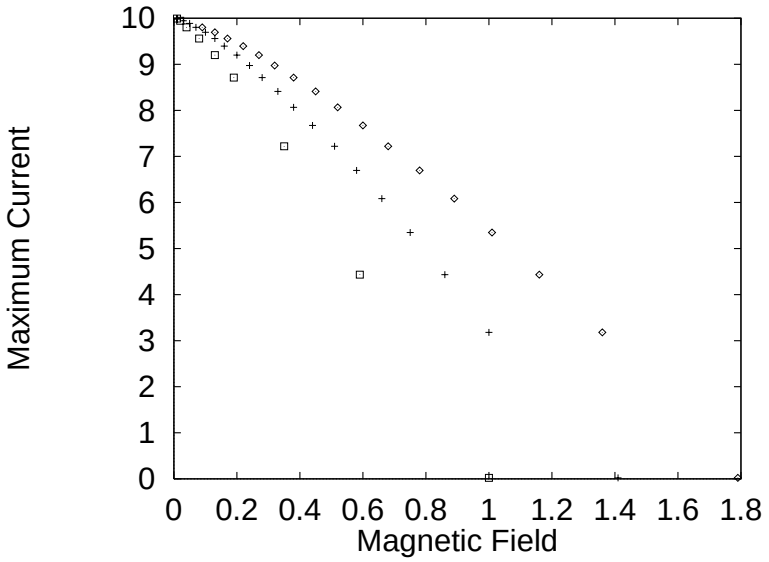

Fig. 8. Plot of the maximum tunneling current as a function of the external magnetic field (overlap geometry) for three different values of $w_0 = 1.2$ (rhombus), 2 (crosses), and 4 (squares).

will vanish. If we lower the current, then we will approach the modes of Fig. 3 as $I \to 0$. The BC for the modal amplitudes are:

$$\left.\frac{dA_m}{dx}\right|_{x=\pm\ell/2} = H \int_{-w_0/2}^{w_0/2} X_n(y)dy\,. \tag{19}$$

In Fig. 8, we plot the maximum current for the overlap geometry with $w_0 = 1.2$, 2.0, and 4.0, and the three curves coalesce at the same current for $H = 0$, since for small $w < 4$, we do not expect saturation effects as in the inline geometry (Fig. 4). The values for H_c should be exactly the same as for the inline geometry and the small difference is, because in the overlap problem, the eigenmodes must be determined numerically and for the sharp jump due to $U(y)$, one needs a very fine grid in discretizing the equations for the amplitudes $A_n(x)$.

In a long junction with overlap current, the waveguide mode frequencies (at $k \to 0$) must be determined numerically. This was achieved by solving numerically Eq. (8) with $\phi_0(y)$ given by Eq. (17).

5. Linear Modes in the Absence of Current

In the absence of losses and driving terms, the small amplitude waves in a long lateral window junction satisfy the equation,

$$\left(\partial_x^2 + \partial_y^2 - \frac{1}{c^2(y)}\partial_t^2\right)\phi = -U(y)\phi \tag{20}$$

which differs from Eq. (1) by the capacitive term, which is different in the window and idle region, i.e., the phase velocity c is y dependent. The phase velocity is

assumed to have the form,

$$c(y) = \begin{cases} 1\,, & \text{in the window} \\ c_i\,, & \text{in the idle region} \end{cases} \tag{21}$$

while $U(y)$ is given in Eq. (2).

We should remark here that the introduction of the dynamic term $-[1/c^2(y)]\partial_t^2$, with different velocities in the two regions does not alter significantly the static properties of the junction. This is because the capacitance of the device depends on the width d of the insulating layer as $C \propto (1/d)$, while the inductance L is proportional to the magnetic thickness, i.e., $L \propto 2\lambda_L + d$, where λ_L is the London penetration depth. However, we consider the case $\lambda_L \gg d$ and the influence on the inductance variation is very small, and we neglect it.

We assume that we have traveling waves in the x-direction with: $\phi(x,y,t) \propto \tilde{\phi}(y)\exp[i(kx-\omega t)]$. Inserting $\phi(x,y,t)$ into Eq. (20), gives,

$$\tilde{\phi}_{yy} = \tilde{\phi}\left(-U(y) + k^2 - \frac{\omega^2}{c^2(y)}\right) \tag{22}$$

with boundary conditions of vanishing current, $\phi_y(y = \pm\,(w_0/2)) = 0$.

In the window $U(y) = -1$, $c(y) = 1$, thus, $\tilde{\phi}_{yy} = (1 + k^2 - \omega^2)\tilde{\phi}$ with solutions,

$$\tilde{\phi} \propto \exp(\pm qy)\,, \quad \text{where} \quad q^2 = 1 + k^2 - \omega^2\,. \tag{23}$$

Similarly, in the idle region, $U(y) = 0$, $c(y) = c_i$, and $\tilde{\phi}_{yy} = [k^2 - (\omega^2/c_i^2)]\tilde{\phi}$, with solutions,

$$\tilde{\phi} \propto \exp(\pm\kappa y)\,, \quad \text{where} \quad \kappa^2 = k^2 - \frac{\omega^2}{c_i^2}\,. \tag{24}$$

The κ and q are the local wavenumbers, in the idle and window regions respectively. They can be either real or imaginary.

To obtain the dispersion relation $\omega(k)$, we must also use the matching conditions at the window — idle region interface (continuity of the phase ϕ and its derivative with respect to y at the interface). From the symmetry of $U(y)$ and $c(y)$, we can separate the normal modes into symmetric and antisymmetric modes.

(i) Symmetric case.

In this case, the solutions in the idle and window regions are:

$$\Psi_0 = A_0 \cosh\left[\kappa\left(y - \frac{w_0}{2}\right)\right]\,, \quad \frac{w}{2} \le y \le \frac{w_0}{2}\,,$$

$$\Phi_1 = A_1 \cosh(qy)\,, \quad |y| \le \frac{w}{2}\,.$$

From the matching interface conditions, we get the eigenvalue equation for $\omega(k)$, given by:

$$q\,\tanh\frac{qw}{2} = \kappa\,\tanh\left(\kappa\frac{w - w_0}{2}\right)\,. \tag{25}$$

This is identical to Eq. (33) in the Appendix, if we put $k = 0$ in the expressions for κ and q.

(ii) Antisymmetric case.

Similarly, we have,

$$\Psi_0 = A_0 \cosh\left[\kappa\left(y - \frac{w_0}{2}\right)\right], \quad \frac{w}{2} \le y \le \frac{w_0}{2},$$

$$\Phi_1 = A_1 \sinh(qy), \quad |y| \le \frac{w}{2}$$

and the corresponding result for the dispersion relation is given implicitly by:

$$q \coth\frac{qw}{2} = \kappa \tanh\left(\kappa\frac{w - w_0}{2}\right). \tag{26}$$

In the earlier analysis, these modes for $k = 0$ were not presented because the phase difference $\phi(x, y)$ to be expanded was a symmetric in y (due to the boundary conditions), and therefore, has no projection on antisymmetric modes.

Numerically, the dispersion relation is obtained by solving the equations,

$$S(k, \omega) = 0, \quad A(k, \omega) = 0$$

where,

$$S = q \tanh\frac{qw}{2} - \kappa \tanh\left(\kappa\frac{w - w_0}{2}\right) \tag{27}$$

$$A = q \coth\frac{qw}{2} - \kappa \tanh\left(\kappa\frac{w - w_0}{2}\right) \tag{28}$$

and we get the symmetric and antisymmetric branches correspondingly.

For $w = w_0$ (no idle region), from $S = 0$ and $A = 0$, the dispersion relation is given by, $\omega(k) = \sqrt{1 + k^2 + (n\pi/w)^2}$, where $n = 0, 1, 2, 3, \ldots$. For relatively large ω, the spacing between the modes at $k = 0$ is $\Delta\omega = n\pi/w$. For $w \neq w_0$, we must solve numerically.

5.1. *Size dependence at long wavelength frequencies $\omega(k = 0)$*

In Fig. 9, we show the dependence of ω at $k = 0$ on the total junction width w_0, for $c_i = 1$ and $w = 1$. We see several branches $\omega_n(k)$ as expected for this complex waveguide structure, which as a function of w_0 for $k = 0$, behave like $\omega_n(0) = \sqrt{1 + (n\pi/w_0)^2}$, where n is integer, when the idle region is small (i.e., $w_0 \simeq w$). For large w_0, we expect the idle region to determine the spectrum, i.e., $\omega_n(0) = c_i(n\pi/w_0)$, and we plot these curves (solid lines) in Fig. 9. We see that, indeed the agreement with the numerical curves is quite good except for the lowest branches. Only for the low lying modes, we see differences with this simple expression, since in that case the barrier in the window (created by the tunneling) becomes significant there. Also, the agreement is better for the odd modes since in that case, ϕ vanishes near the center so that the tunneling term does not contribute,

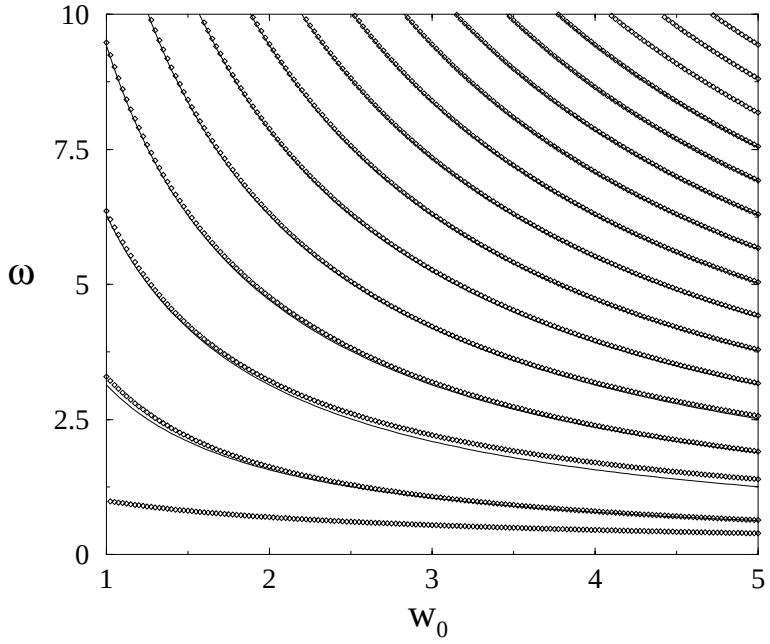

Fig. 9. Frequency spectrum versus w_0 at $k = 0$ with $c_i = 1$ and $w = 1$. The solid curves are given by $\omega = c_i \pi n / w_0$, for $n = 1, 2, \ldots$ ($n = 0$ coincides with x-axis).

because the simple expression neglects the window tunneling. On the other hand, for the even modes we expect the tunneling term to contribute.

In the case where $c_i \neq 1$, things become more complicated. In Fig. 10, we give the branches $\omega_n = \omega_n(0)$ for $c_i = 2$ and $w = 1$, as a function of w_0 along with the curves $\omega_n = c_i(n\pi/w_0)$, $n = 1, 2, \ldots, 10$, which is the result when the window can be neglected. As one can see in this figure, some branches fit very well in the curves with n odd. These branches correspond to the antisymmetric modes. The branches corresponding to the symmetric modes, as w_0 increases, they leave the curves $\omega = c_i(n\pi/w_0)$, n even, moving toward the antisymmetric branches. For very large w_0, they eventually coincide. This can be seen from Eqs. (27) and (28). For w_0 very large, we can neglect w in the argument of the second term of the right hand side of Eq. (27). Thus, we get, for the symmetric modes,

$$q \tanh \frac{qw}{2} - \tilde{\kappa} \tan\left(\tilde{\kappa}\frac{w_0}{2}\right) = 0\,. \tag{29}$$

Then, we define the small parameter $\epsilon = 1/w_0$ and assume that $\tilde{\kappa} = [(2n+1)\pi + \delta]/w_0$, where δ is assumed to be a small number, which in fact depends on w_0 as $\delta \sim 1/w_0$ (so it is of the same order as ϵ). We assume that $\tilde{\kappa}$ for the symmetric $2n$ mode is very close to the value for the antisymmetric $2n+1$ mode as suggested by the numerical results and we check for consistency in order to determine δ. We rewrite $\tilde{\kappa}$ as $\tilde{\kappa} = \epsilon(\pi + \delta)$ for the choice of $n = 0$ and one can get the similar results for every n. Then from Eq. (23) and the value for $\tilde{\kappa}$ above, we get $q \simeq 1 - (c_i^2 \epsilon^2 \pi^2/2)$.

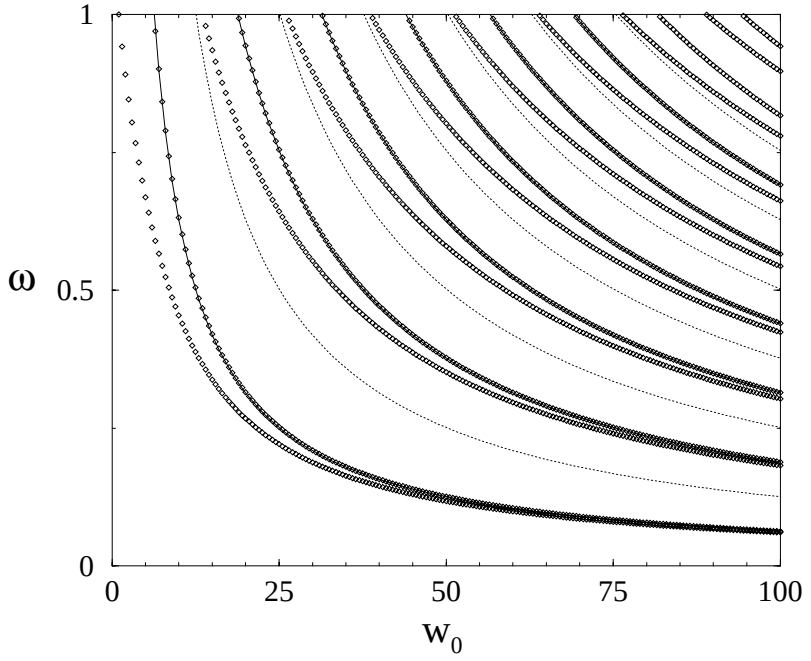

Fig. 10. Frequency spectrum versus w_0 at $k = 0$ with $c_i = 2$ and $w = 1$. The curves shown are given by $\omega = c_i \pi n / w_0$, for n integer. Solid curves: n odd, dashed curves: n even.

We expand $\tanh(qw/2)$ around $q = 1$ in powers of the small quantity $c_i^2 \epsilon^2 \pi^2 / 2$, and we get,

$$\tanh \frac{qw}{2} \simeq \tanh \frac{w}{2} - \frac{w c_i^2 \epsilon^2 \pi^2}{4} \operatorname{sech}^2 \frac{w}{2} .$$

The expansion of $\tan(\tilde{\kappa} w_0 / 2)$ gives,

$$\tan\left(\frac{\tilde{\kappa} w_0}{2}\right) \simeq -\frac{2}{\delta}\left(1 - \frac{\delta^2}{12}\right) .$$

Introducing the expressions for $\tilde{\kappa}$, q, $\tanh(qw/2)$, $\tan(\tilde{\kappa} w/2)$ into Eq. (29), and keeping the terms up to first order in ϵ, δ and their combinations, we get,

$$\delta_s \simeq -\frac{2\epsilon\pi}{\tanh \dfrac{w}{2}} .$$

Following the same steps, we get from Eq. (28) for the antisymmetric modes that:

$$\delta_a \simeq -2\epsilon\pi \tanh \frac{w}{2} .$$

These results are consistent with our assumption that both $\delta \sim 1/w_0$. Both solutions are negative, in agreement with the numerical data, while the antisymmetric is closer to the curve $\omega = c_i \pi / w_0$. When $w_0 \to \infty$, the two solutions coincide, and ω gets exactly the value $c_i \pi / w_0$.

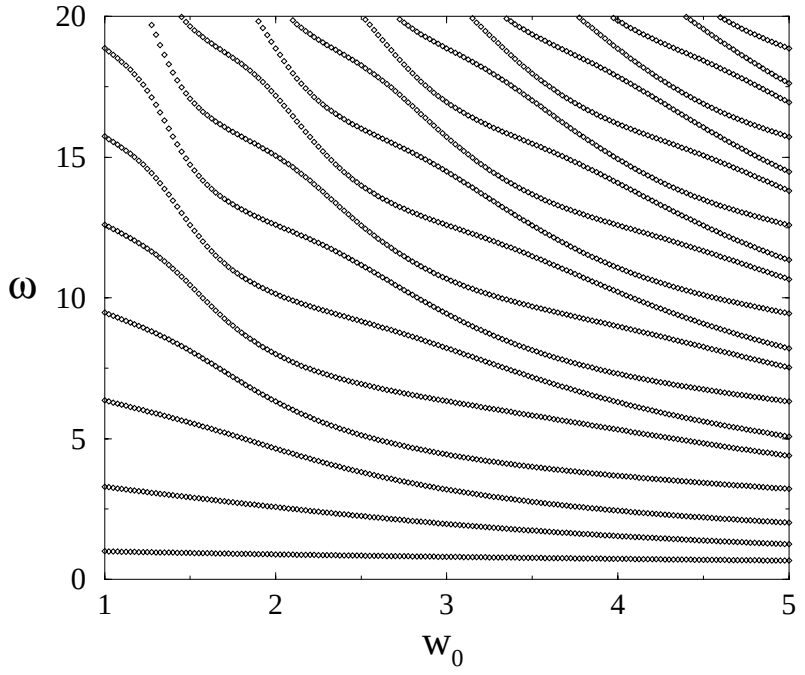

Fig. 11. Frequency spectrum versus w_0 as in Fig. 10 but on a different scale.

In Fig. 11, we show the branches $\omega_n = \omega_n(0)$ for the parameters we used in the previous figure, but on a different scale. Here, one can see that the picture is rather complicated, since there is some interaction among the various branches. Apparently, the branches attract and repel each other. Thus, two branches show a maximum and minimum distance at specific points, which depend on the velocity c_i. In Fig. 12, we show a rather extreme case, $c_i = 100$, where there is high velocity contrast in the two (window and idle) regions. Here, the branches $\omega = \omega(0)$ are flat everywhere (independent of w_0) and $\omega(0) = \sqrt{1 + (n\pi/w)^2}$, $n = 0, 1, 2, \ldots$, except close to the curves $\omega = c_i m\pi/(w_0 - w)$, where m is odd integer. Close to these resonance curves, there is a sudden change. By approaching the first resonance curve ($m = 1$), a branch, say $\omega_n(0)$, decreases fast. It crosses the resonant curve, still decreasing, and then it takes the position of the $\omega_{n-2}(0)$ branch, becoming flat again (until it reaches the second resonance curve where it becomes $\omega_{n-4}(0)$, and so on). This can be seen more clearly in Fig. 13, which is a magnified part of Fig. 12.

Here, only three branches for clarity, those for $n = 7, 8$, and 9 are shown. The curve $\omega = c_i\pi/(w_0 - w)$ crosses the three branches each at a single point. This point is located at a specific w_0, which is given by:

$$c_i \frac{m\pi}{w_0 - w} = \sqrt{1 + \left(\frac{n\pi}{w}\right)^2}.$$

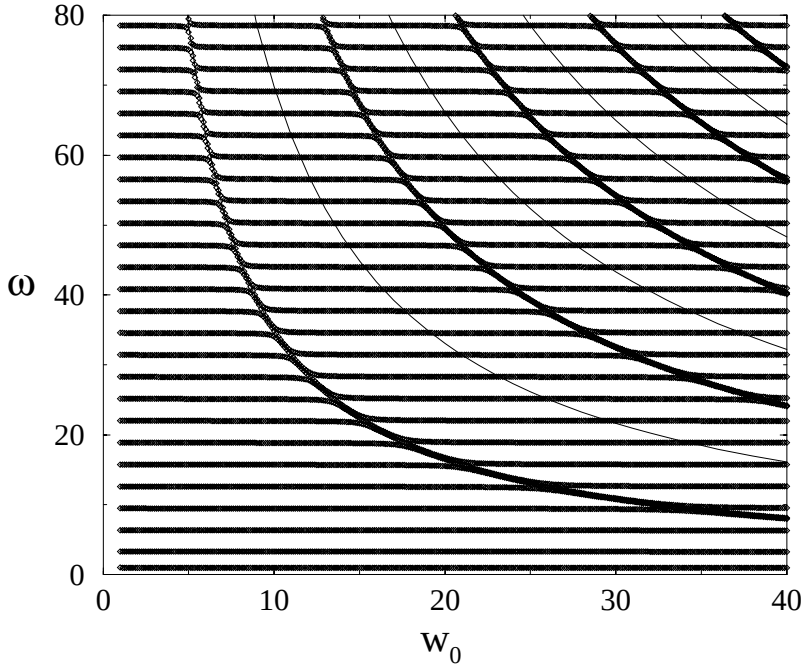

Fig. 12. Frequency spectrum versus w_0. $c_i = 100$, $w = 1$, and $k = 0$. The curves shown are given by $\omega = c_i m\pi/(w_0 - w)$. The resonance curves correspond to m odd.

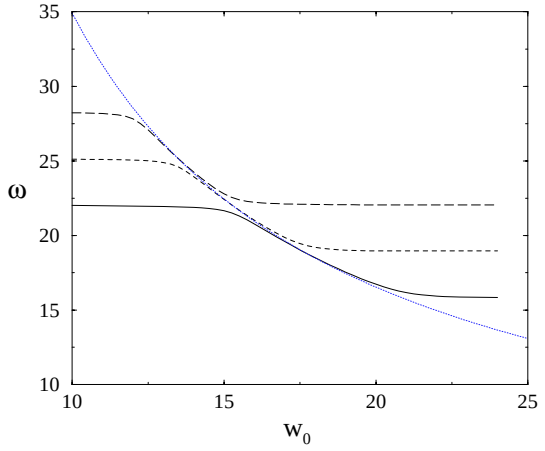

Fig. 13. Frequency spectrum versus w_0 as in Fig. 12 but on finer scale. Solid curve: $n = 7$, dashed curve: $n = 8$, long-dashed curve: $n = 9$, and dotted curve: $\omega = c_i\pi(w_0 - w)(m = 1)$.

Near these crossing points, the slope of the dispersion curve is almost the same as that of the resonance curves. The resonance point with the lowest frequency ω is shown in Fig. 14. This is at $w_0 \simeq 314$, for these parameters. We should also note that each time a branch $\omega_n(0)$ crosses a resonance curve, two of the nodes of the

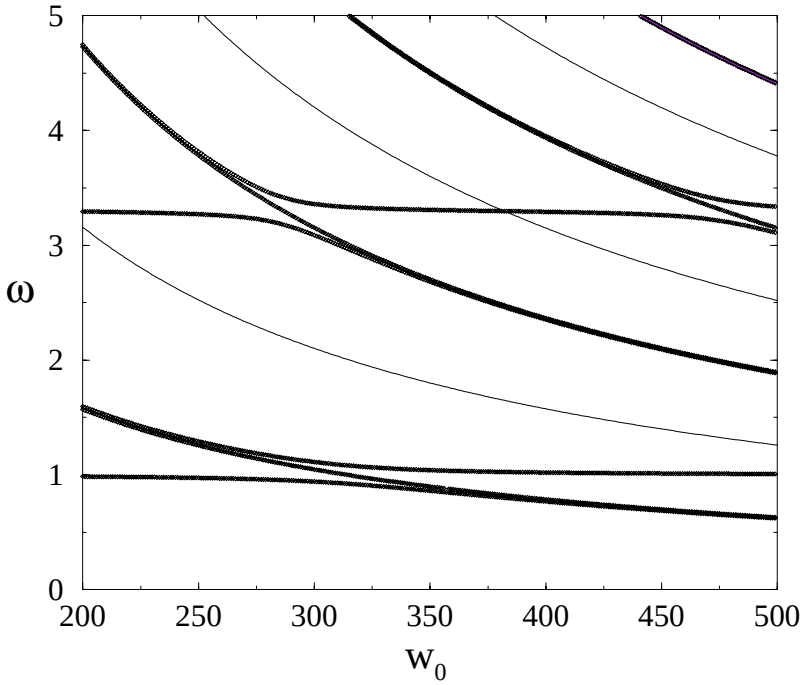

Fig. 14. Frequency spectrum versus w_0 as in Fig. 12 but for large w_0. The curves shown are given by $\omega = c_i m\pi/(w_0 - w)$. The resonance curves correspond to m odd (they are completely covered by the points).

corresponding eigenmode leave the window region and appear in the idle region. We also plot (solid lines) the modes $\omega_n = c_i n\pi/(w_0 - w)$ which for odd n, coincide with the numerical results in the scale used, and are not seen.

5.2. *Wavevector dependence* $\omega(k)$

Now, we turn to the dependence of ω on k. We choose $w_0 = 2$, $w = 1$, and look at four different values of the velocity c_i which correspond to four different patterns. In Fig. 15, the velocity $c_i = 0.5$. Below the line $\omega = k$ where q is real, the symmetric and antisymmetric branches coincide. Not very far, but below this line, q is large enough that $\tanh q$ can be considered to be practically unity. Then, the equations $S = 0$ and $A = 0$ give indeed identical solutions, as seen in Eqs. (27) and (28). Below $\omega = k$, the branches $\omega = \omega(k)$ fit with the curves $\omega(k) = c_i\sqrt{k^2 + \tilde{\kappa}_n^2}$, where $\tilde{\kappa}_n$ is approximately given by $\beta k \simeq \tilde{\kappa}_n \tan(\tilde{\kappa}_n/2)$, and $\beta = \sqrt{1 - c_i^2}$. The point $c_i = 0.5$ is a particular one, where the frequencies at $k = 0$ are grouped three together (except the lowest two), the middle of which is at $\omega = n\pi$ with $n = 1, 2, 3, \ldots$, where odd (even) n corresponds to antisymmetric (symmetric) modes. The two neighbors (which are of opposite symmetry from the central one) are given approximately by $\tan\omega = \pm c$, where in this case $c \simeq 1.118$.

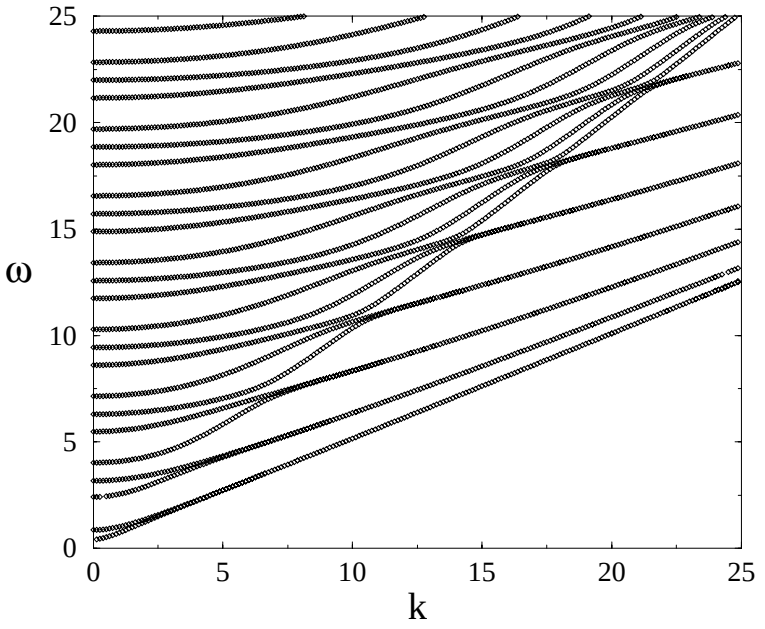

Fig. 15. Frequency spectrum versus k. $c_i = 0.5$, $w = 1$, and $w_0 = 2$.

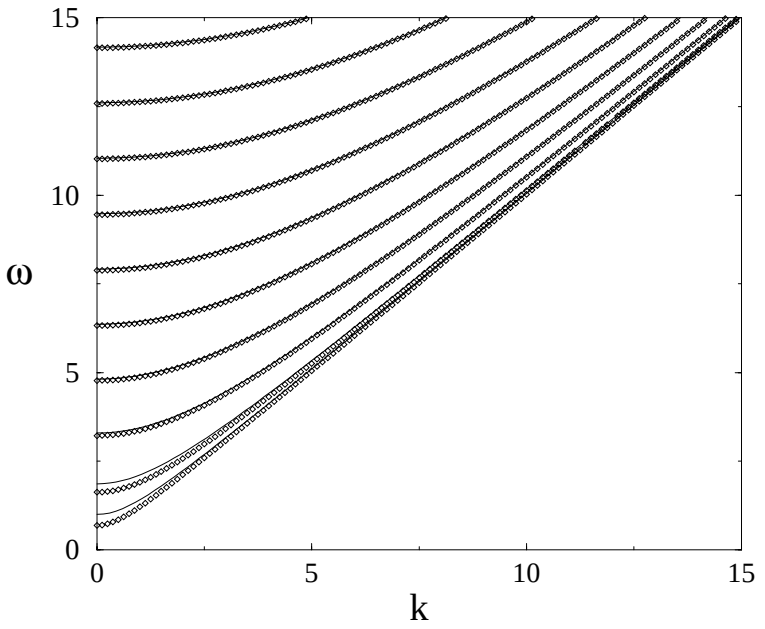

Fig. 16. Frequency spectrum versus k. $c_i = 1$, $w = 1$, and $w_0 = 2$. The solid curves are given by $\omega_n(k) = \sqrt{1 + k^2 + \tilde{q}^2}$, where $\tilde{q} = (n\pi/w_0)$.

In Fig. 16, the velocity is $c_i = 1$. If we assume that $\tilde{q}_n w + \tilde{\kappa}_n(w_0 - w) = n\pi$, where n is integer and the $\tilde{\kappa}$ and $\tilde{q}$ are defined as $\kappa = i\tilde{\kappa}$ and $q = i\tilde{q}$ respectively, then we get from $S = 0$ and $A = 0$ so that,

$$\tilde{q} \simeq \begin{cases} \dfrac{2n\pi}{w_0} \\ \dfrac{(2n+1)\pi}{w_0} \end{cases}$$

respectively, for relatively large ω. Then $\omega(k) = \sqrt{1 + k^2 + \tilde{q}^2}$.

In Fig. 17, $c_i = 2$. In the same way as in the case where $c_i = 0.5$, we can assume that little below the line $\omega = c_i k$ where κ is real, it is also large enough that $\tanh(\kappa/2) = 1$. Then, $\omega(k) = \sqrt{1 + k^2 + \tilde{q}^2}$, where $\tilde{q}$ is given by (approximately) $\tan \tilde{q}w \simeq -2\tilde{q}/k[1 - (1/c_i^2)]$. Here, one can also prove that the slope of the branches at the resonance points [that is, where $1 + k^2 + \tilde{q}^2 = c_i^2(k^2 + \tilde{\kappa}_n^2)$] is equal to c_i. In this case, the symmetric and the antisymmetric solutions do not merge at high k. The solid line shown in the figure is $\omega(k) = c_i\sqrt{k^2 + [\pi/(w_0 - w)]^2}$. Finally, in Fig. 18, the velocity is $c_i = 100$. Here, the branches change smoothly, and at $k = 0$, the frequencies are $\omega(0) = \sqrt{1 + (n\pi/w)^2}$, where $n = 0, 1, 2, \ldots$.

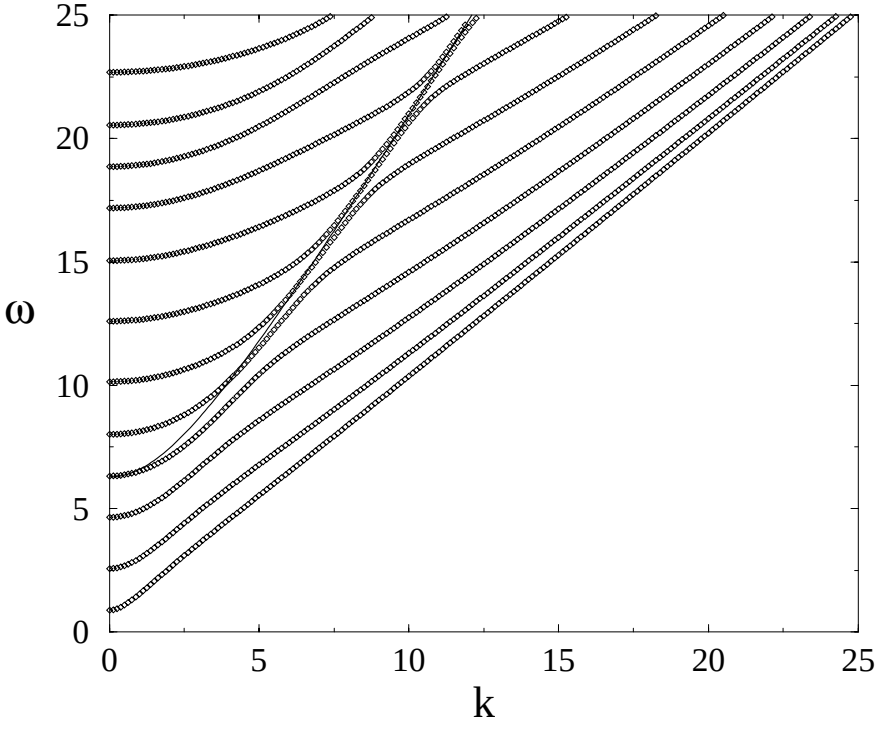

Fig. 17. Frequency spectrum versus k. $c_i = 2$, $w = 1$, and $w_0 = 2$. The solid line is given by $\omega = \sqrt{k^2 + [\pi/(w_0 - w)]^2}$.

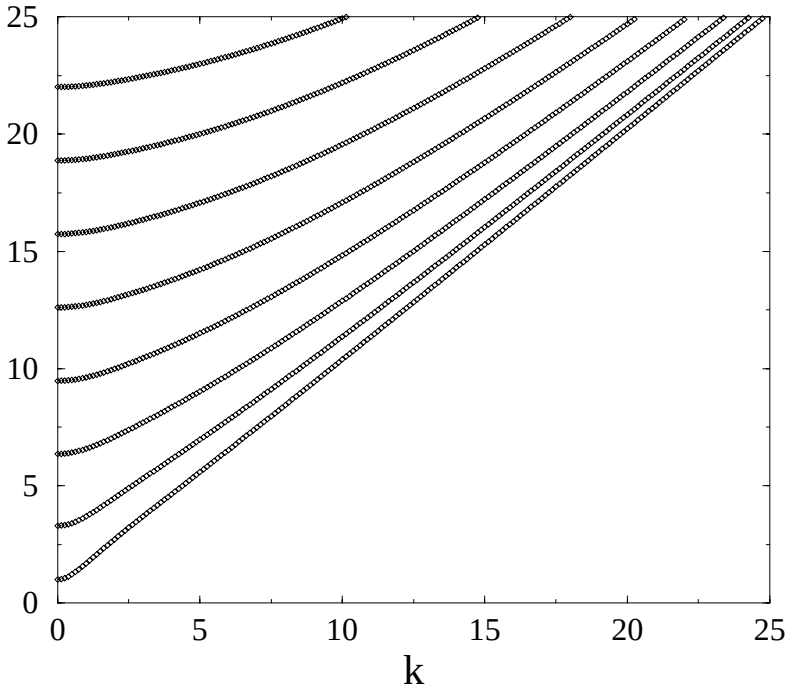

Fig. 18. Frequency spectrum versus k. $c_i = 100$, $w = 1$, and $w_0 = 2$.

6. Conclusion

We presented an efficient procedure to evaluate the electromagnetic response of a lateral window device, which can be considered as a coupled system of an active waveguide (tunneling window) and a passive one (idle region with no tunneling). We see that the effect of the passive region is to change the characteristic length for flux variation. We compared with simple estimates for the fluxon width and the effective length. The procedure can be extended to relatively large w_0 without a considerable increase in the number of modes in the expansion. The introduction of the auxiliary function ϕ_0 and the linearized mode expansion reduces the solution of a PDE problem into a small system of ODE's. We see that in the inline geometry, the maximum current increases linearly with the characteristic length and the critical magnetic field inversely with it. For the overlap geometry, the critical magnetic field is the same as in the inline, while the $I_{\max}(0)$ is independent of w_0. We also see that the eigenvalues in the problem for the expansion modes $X_n(y)$ correspond to the squared frequency of the long wavelength waveguide modes. These frequencies vary with the overlap bias current.

We gave the dispersion relation for the waveguide modes and presented a simple explanation for its variation with the geometric parameters. This is done for the case where we have a variation normal to the waveguide, both of the critical current

and the linear Swihart velocity. The calculations can be easily extended to the case where we have an overlap current. In that case, the linear waves are perturbations around $\phi_0(y)$, which is given implicitly in Eq. (17). The modes are given by the eigenvalue problem in Eq. (8). Now, we have the possibility to strongly modify the lowest branches of the dispersion and in a way that is of interest for applications. One of the properties of this waveguide structure is to act as a high pass filter with a lower cutoff at $\omega_1(k = 0)$, i.e., no waves can propagate for $\omega < \omega_1(0)$. In this case, the cutoff which depends on the geometry can also be varied with the overlap bias current in a continuous way. In fact, if we use the maximum overlap current at $H = 0$, then there is no low frequency gap in the spectrum. In our study, we have considered the case of zero damping which is a realistic assumption for temperatures much lower than the critical temperature. At high frequencies, a small damping can be taken into account by considering a complex propagation parameter with a small imaginary part. This will be a weak perturbation on the spectrum results.

Acknowledgment

Y. G. and J. G. C. acknowledge the hospitality of the University of Crete. The visit of J. G. C. was made possible by a grant under the Greek-French collaboration agreement and that of Y. G. by a grant from the University of Crete. Y. G. received partial support from the grant K95100 of the International Science Foundation and the Government of Ukraine and from SRC QM "Vidhuk".

Appendix

In the case that $\phi_0 = 0$, we must solve the eigenvalue problem,

$$-X_n''(y) - U(y)X_n = \lambda_n X_n\,, \tag{30}$$

in the range $y\epsilon[-(w_0/2), (w_0/2)]$ with the BC,

$$\left.\frac{dX_n}{dy}\right|_{\pm w_0/2} = 0\,. \tag{31}$$

For $\lambda < 1$, we put $\lambda_n = \kappa_n^2$ and write the solution in the window and idle region (assuming y-symmetry) as:

$$\begin{aligned} X_n^W(y) &= A_1 \cosh(\sqrt{1-\kappa_n^2}y) |y| \le w/2\,, \\ X_n^I(y) &= \ A_2 \cos[\kappa_n(|y| - w_0/2)] w/2 \le |y| \le w_0/2 \end{aligned} \tag{32}$$

Matching at the interface on $y = \pm w/2$, gives the equation for the eigenvalues,

$$\sqrt{1-\kappa_n^2}\tanh\left(\sqrt{1-\kappa_n^2}\frac{w}{2}\right) = -\kappa_n \tan\left[\frac{\kappa_n}{2}(w - w_0)\right] \tag{33}$$

while normalizing we have,

$$A_1 = \left\{ \frac{1}{2} \left[w + \frac{\sinh(C_n w)}{C_n} + \left(\frac{\cosh\left(C_n \frac{w}{2}\right)}{\cos(\kappa_n w')} \right)^2 \left(2w' + \frac{1}{\kappa_n} \sin(2\kappa_n w') \right) \right] \right\}^{-1/2} \quad (34)$$

$$A_2 = A_1 \left[\frac{\cosh\left(C_n \frac{w}{2}\right)}{\cos(\kappa_n w')} \right], \quad (35)$$

with,

$$w' = \frac{w_0 - w}{2} \quad \text{and} \quad C_n = \sqrt{1 - \kappa_n^2}.$$

For $\lambda > 1$, we can obtain directly by letting $\sqrt{1-\kappa_n^2} \to \sqrt{\kappa_n^2 - 1}$ and $\cosh \to \cos$, $\sinh \to \sin$, $\tanh \to \tan$.

If the value of $\phi_0 = \pi$ is chosen, then we have a change of sign in the term with $U(y)$, which now acts like a well. All the previous expressions can be taken by a simple analytic continuation. The convergence for $\phi_0 = 0$, however is much faster.

References

1. A. Barone and G. Paterno, *Physics and Applications of the Josephson effect* (John Wiley, 1982).
2. J. G. Caputo, N. Flytzanis, and M. Devoret, *Phys. Rev. B* **50**, 6471 (1994).
3. J. G. Caputo, N. Flytzanis, and E. Vavalis, *Int. J. Mod. Phys. C* **6**, 241 (1995).
4. J. G. Caputo, N. Flytzanis, Y. Gaididei, and E. Vavalis, *Phys. Rev. E* **54**, 2092 (1996).
5. C. S. Owen and D. Scalapino, *Phys. Rev.* **164**, 538 (1967).
6. J. G. Caputo, N. Flytzanis, and E. Vavalis, *Int. J. Mod. Phys. C* **7**, 241 (1996).
7. R. P. Huebener, *Rep. Prog. Phys.* **47**, 175 (1984).
8. M. Abramowitz and I. A. Stegun, *Handbook of Mathematical Functions* (Dover Publications, Inc., New York, 1972).